AIAA/AAS Astrodynamics Specialist Conference and Exhibit
21 - 24 August 2006, Keystone, Colorado

AIAA 2006-6398

Keystone Colorado, August 21–24, 2006

AIAA-2006-6398

Covariance Analysis of Cassini Titan Flyby using SAR and Altimetry Data

Ryan S. Park *
The University of Michigan, Ann Arbor, Michigan, 48109
L. Alberto Cangahuala, † Paul C. Chodas, ‡ and Ian M. Roundhill §
Jet Propulsion Laboratory, Pasadena, California, 91109

The Cassini spacecraft is equipped with a radar system that provides Synthetic Aperture Radar (SAR) and altimetry data types for scientific purposes. The radar operates in these modes during close flybys of Titan; due to operations constraints, ground-based radiometric navigation data are unavailable. This paper discusses a covariance study of Titan flybys using both SAR and altimetry data as additional navigation observables and show the possibility of improving the trajectory reconstruction during these flybys. Realistic measurement accuracies and trajectory model are considered; the result that there is a possible improvement of planar motion estimation by an order of magnitude.

I. Introduction

Synthetic Aperture Radar (SAR) is an important remote sensing technique for characterizing topography, especially in areas that are obscured by clouds.[1] Poor knowledge of the radar paths above the terrain during the campaign can compromise the conversion of the radar return information into elevation profiles and maps. In spacecraft SAR applications independent systems, such as GPS, can be used to determine the spacecraft orbit to a fidelity such that remaining errors do not introduce artifacts into the derived terrain models. For SAR applications beyond the Earth, these systems are not readily available, and spacecraft operating conditions make it difficult, if not impossible, to perform radiometric tracking concurrently with the SAR passes. However, the SAR data (as well as altimetry) collected during these passes has sufficient geometric strength to improve the spacecraft trajectory with respect to the target, as well as improve the rotational modeling of the target. A multi-mission capability to routinely process the SAR and altimetry data as part of orbit determination process would enhance science returns at these bodies, and could be used for SAR-like applications at other obscured solar system target regions.

To date, there have been SAR applications for terrain modeling at two targets beyond the Earth: Venus (most recently through the Magellan mission) and Titan (through Cassini's ongoing Titan flybys). Chodas *et al.*[2,3] used landmarks common to multiple SAR passes together with ground-based Doppler measurements to tie the corresponding orbit arcs together. Each SAR/landmark measurement was then used to estimate the corresponding topographic landmark and any redundant information content, if it existed, was fitted to estimate the other variables, i.e., spacecraft state, rotation rate, pole location, etc. In different perspective, one can think of each SAR landmark playing a role similar to that of a fixed tracking station (or a transponder) on Venus. An institutional navigation software at that time was augmented to incorporate the SAR data

*Graduate Student Research Assistant, PhD Candidate, Department of Aerospace Engineering, The University of Michigan, Ann Arbor, Michigan, sanghp@umich.edu
†Deputy Manager, Guidance, Navigation and Control, Jet Propulsion Laboratory, Pasadena, California
‡Senior Member of Engineering Staff, Solar System Dynamics Group, Jet Propulsion Laboratory, Pasadena, California
§Member of Technical Staff, Outer Planet Navigation Group, Jet Propulsion Laboratory, Pasadena, California

type. As the next step in establishing a more general capability, the Magellan SAR data were reprocessed with the current navigation software set. Improvements in measurement and dynamic modeling have resulted in improved SAR pre- and post-fit data residuals. Using this data as a test case, the filter setup was then ported to JPL's next generation navigation software, Mission-analysis, Operations, and Navigation Toolkit Environment (MONTE) and the results were repeated.

The following step in the plan was to examine the Cassini/Titan SAR/altimetry data set and understand the opportunities that it could provide. Although it is not possible to perform a SAR campaign with regularly spaced swaths as was the case with Magellan, swath overlaps between different flybys are expected during the prime mission. In addition, the altimetry data are being collected during each pass. We present a covariance analysis to stress the benefits of short arc Cassini SAR overlaps and altimeter passes. The result shows that there is roughly an order of magnitude improvement in the spacecraft relative ephemeris knowledge in the orbit arc plane from processing the currently available radar measurements and the cross-track uncertainty can be improved when overlapping SAR swaths are obtained in the future.

II. Covariance Analysis

A. Motivation

The Cassini spacecraft (Figure 1), which was inserted into the Saturnian system in 2004, has, so far, performed several SAR observations at Titan. Figure 2 depicts the currently available SAR swaths,[4] and apparently, no overlapping SAR swaths have yet been obtained. The SAR data becomes significant only when each landmark is observed in at least two different swaths, where the second observation occurs at a later time. It must be observed twice because most of the data information contents from the first measurement is fitted to estimate the landmark location, and a long time duration is necessary since the velocity covariance is, in a sense, inversely proportional to the time difference. For example, consider a simple example $r = vt$. The velocity uncertainty is simply $\sigma_v = \sigma_r/t$ and the advantage of the long time interval is obvious. Hence, dynamic parameters, such as rotation rate, can be estimated to a high precision by processing the SAR/landmark data. However, since overlapping swaths are not currently available we turn to a covariance analysis in order to characterize the expected level of precision by processing the actual altimetry and SAR measurements. In this study, only the spacecraft state estimation is considered since our primary purpose is to implement these data types as additional navigational observables for trajectory navigation at bodies with obscured atmosphere.

B. Initial State Analysis Formulation

A covariance (sensitivity) analysis is often used as a design tool to understand the performance of a filter.[5,6,7,8] It is based on the least-squares principle and the problem can be posed either in a batch or in a sequential mode. In this study we consider the batch process (initial state analysis) and assume negligible process noise (unmodeled acceleration) since the data arc we consider is over a relatively short time frame ($\sim$ 1 hour). Note that, under this assumption, the batch and sequential methods yield the same result. The rest of this section briefly discusses the basics of a covariance analysis.

First define a cost function J as

$$J = \frac{1}{2}\sum_{k=1}^{N}\frac{1}{\sigma_k^2}\left[\mathbf{z}_k^* - \mathbf{z}_k(\mathbf{y}_0)\right]^2 \tag{1}$$

where N is the number of measurements, σ_k is the measurement noise uncertainty, $\mathbf{z}_k^*$ is the actual measurement, and $\mathbf{z}_k$ is the predicted measurement. In the batch process the state to be estimated is usually stated as

$$\mathbf{y}_0 = \begin{bmatrix} \mathbf{x}_0^T & \mathbf{p}^T & \mathbf{q}^T \end{bmatrix}^T \tag{2}$$

where $\mathbf{x}_0$ is the epoch spacecraft state vector (T represents a transpose), $\mathbf{p}$ is the dynamics parameter vector, and $\mathbf{q}$ is the measurement model parameter vector with dimensions n, m, and l, respectively. The goal of the least-squares approximation is to minimizes the cost function J in order to fit $\mathbf{y}_0$ to the data. After applying the necessary conditions to J and linearizing the nominal values of $\mathbf{y}_0$, we obtain the following

normal equation:

$$\sum_{k=1}^{N} \frac{1}{\sigma_k^2} \left(\frac{\partial \mathbf{z}_k(\mathbf{y}_0)}{\partial \mathbf{y}_0} \right)^T [\mathbf{z}_k^* - \mathbf{z}_k(\mathbf{y}_0)] = \left[\sum_{k=1}^{N} \frac{1}{\sigma_k^2} \left(\frac{\partial \mathbf{z}_k(\mathbf{y}_0)}{\partial \mathbf{y}_0} \right)^T \left(\frac{\partial \mathbf{z}_k(\mathbf{y}_0)}{\partial \mathbf{y}_0} \right) \right] \delta \mathbf{y}_0 \tag{3}$$

where the epoch state information matrix is defined as

$$\mathbf{\Lambda}(t_0; t_N, t_0) = \sum_{k=1}^{N} \frac{1}{\sigma_k^2} \left(\frac{\partial \mathbf{z}_k(\mathbf{y}_0)}{\partial \mathbf{y}_0} \right)^T \left(\frac{\partial \mathbf{z}_k(\mathbf{y}_0)}{\partial \mathbf{y}_0} \right) \tag{4}$$

$$= \sum_{k=1}^{N} \frac{1}{\sigma_k^2} \mathbf{\Phi}^T(t_k, t_o) \mathbf{H}_k^T \mathbf{H}_k \mathbf{\Phi}(t_k, t_o) \tag{5}$$

Here $\mathbf{H}_k$ is the measurement partial computed at time t_k and $\mathbf{\Phi}(t_k, t_0)$ is the usual state transition matrix (STM) mapping the deviations from t_0 to t_k,[9,10] i.e.,

$$\mathbf{H}_k = \left. \frac{\partial \mathbf{z}}{\partial \mathbf{y}} \right|_{t_k} \tag{6}$$

$$\mathbf{\Phi}(t_k, t_0) = \frac{\partial \mathbf{y}(t_i)}{\partial \mathbf{y}(t_0)} \tag{7}$$

where the differential equation for the STM is

$$\dot{\mathbf{\Phi}}(t_k, t_0) = \mathbf{A} \mathbf{\Phi}(t_k, t_0) \tag{8}$$

$$\mathbf{A}(t) = \frac{\partial}{\partial \mathbf{y}} \left(\frac{d\mathbf{y}}{dt} \right) \tag{9}$$

and the initial condition, $\mathbf{\Phi}(t_0, t_0)$, is simply an identity matrix. Note that $\mathbf{\Lambda}_0 = \mathbf{\Lambda}(t_0; t_N, t_0)$ means the information matrix computed at time t_0 after processing all the measurements in the time interval $[t_0, t_N]$.

If we consider $\mathbf{y}_0$ as a Gaussian random vector with a mean, $\bar{\mathbf{y}}_0$, and a covariance matrix, $\mathbf{P}_0$, the probability density function (pdf) can be defined as

$$p(\mathbf{y}_0) = \frac{1}{(2\pi)^{(n+m+l)/2} \sqrt{\det \mathbf{P}_0}} \exp \left[-\frac{1}{2} (\mathbf{y}_0 - \bar{\mathbf{y}}_0)^T \mathbf{P}_0^{-1} (\mathbf{y}_0 - \bar{\mathbf{y}}_0) \right] \tag{10}$$

where the covariance matrix of $\mathbf{y}_0$ is simply

$$\mathbf{P}_0 = \mathbf{\Lambda}_0^{-1} \tag{11}$$

The probability of the state vector $\mathbf{y}_0$ in some volume $\mathcal{B}_0$ is then stated as

$$\Pr(\mathbf{y}_0 \in \mathcal{B}_0) = \int_{\mathcal{B}_0} p(\mathbf{y}_0') d\mathbf{y}_0' \tag{12}$$

Note that, in case of one-dimensional problem, the probability of the random variable in 3-σ ellipsoid yields 99.7 percent.

The direct computation of a matrix inversion in Eqn. (11), however, often introduces numerical errors. In order to retain the numerical precision, we have implemented the Square Root Information Filter (SRIF) algorithm:[9,11]

$$\mathbf{\Lambda}(t_0; t_k, t_0) = \mathbf{R}^T(t_0; t_k, t_0) \mathbf{R}(t_0; t_k, t_0) \tag{13}$$

Here $\mathbf{R}(t_0; t_k, t_0)$ is the initial state SRIF matrix which we propagate, instead of the information matrix, to update data in each time increment. The SRIF matrix is related to the adjoint of the STM and ideally maps to the current time as

$$\mathbf{R}(t_k; t_k, t_0) = \mathbf{R}(t_0; t_k, t_0) \mathbf{\Phi}(t_0, t_k) \tag{14}$$

Let $\mathbf{T}_H$ be an orthogonal Householder transformation matrix such that the updated SRIF matrix is defined as

$$\mathbf{R}(t_0;t_{k+1},t_0) \;=\; \mathbf{T}_H \begin{bmatrix} \mathbf{R}(t_0;t_k,t_0) \\ \sigma_{k+1}^{-1}\mathbf{H}_{k+1}\mathbf{\Phi}(t_{k+1},t_0) \end{bmatrix} \;=\; \begin{bmatrix} \mathbf{R}_H(t_0;t_{k+1},t_0) \\ 0 \end{bmatrix} \tag{15}$$

where $\mathbf{R}_H$ is an upper triangular matrix. In the actual computation, we adopt QR-factorization as the Householder transformation.[9,11] After applying the Householder transformation, the updated information matrix becomes

$$\mathbf{\Lambda}(t_0;t_{k+1},t_0) \;=\; \mathbf{R}_H^T(t_0;t_{k+1},t_0)\mathbf{R}_H(t_0;t_{k+1},t_0) \tag{16}$$

and the updated covariance matrix is

$$\mathbf{P}(t_0;t_{k+1},t_0) \;=\; \mathbf{\Lambda}^{-1}(t_0;t_{k+1},t_0) \;=\; \mathbf{R}_H^{-1}(t_0;t_{k+1},t_0)\mathbf{R}_H^{-T}(t_0;t_{k+1},t_0) \tag{17}$$

which represents the evolution of the *a priori* uncertainties in $\mathbf{y}_0$. Each component in the covariance matrix ($\mathbf{P}_{ij}=\sigma_{ij}$) represents either the covariance of the state or the correlation between two estimated variables. Hence, we can obtain the uncertainty estimates (i.e., standard deviations) of $\mathbf{y}_0$ by computing $\sigma_i=\sqrt{\sigma_{ii}}$, for $i=1\cdots n+m+l$.

Lastly, in case a current state covariance matrix needs to be computed, the initial state covariance matrix, $\mathbf{P}_0$, can be mapped to time t_k as

$$\mathbf{P}(t_k;t_k,t_0) \;=\; \mathbf{\Phi}(t_k,t_0)\mathbf{P}(t_0;t_k,t_0)\mathbf{\Phi}^T(t_k,t_0) \tag{18}$$

and the pdf remains Gaussian since it is invariant under linear operations.

III. Trajectory Dynamics and Measurement Models

A. Trajectory Description

As a nominal trajectory we consider the Cassini T8 Titan flyby, which occurred on October 28, 2005,[4] and the post-processed SAR swath is shown in Figure 3. The initial spacecraft state (32 minutes prior to the periapsis passage) is found from JPL's HORIZONS system[12] and Figure 4 shows the nominal hyperbolic trajectory in Titan-centric frame. The trajectory is propagated via the two-body dynamics

$$\ddot{\mathbf{r}} \;=\; -\frac{\mu_T}{|\mathbf{r}|^3}\mathbf{r} \tag{19}$$

where $\mathbf{r}$ represents the spacecraft position vector and μ_T=8978.03 km^3/s^2 is Titan's GM. For the problem considered in this study, the two-body relation is a reasonably good approximation since the data arc we consider starts from 32 minutes prior to the periapsis passage (P–32 minutes) and ends at 32 minutes after the periapsis passage (P+32 minutes), resulting in a relatively short data arc of 64 minutes. Note that 'P' represents the periapsis of the T8 flyby. The orbit elements of the nominal trajectory are given in Table 1.

Table 1. The nominal trajectory orbital elements

Semi-major axis, a	−292.6 km
Eccentricity, e	14.42
Inclination, i	178.8 deg
Argument of periapsis, ω	86.0 deg
Argument of ascending node, Ω	162.2 deg

As noted earlier, no Earth-based radiometric measurements are available due to planned science activities during the close flybys. We assume that the trajectory reconstruction is available from processing the pre- and post-flyby ground tracking data and used *a priori* state uncertainties of 100 m for the position components and 10 mm/s for the velocity components.

B. Measurement Schedule

The Cassini spacecraft (Figure 1) is equipped with a sophisticated Ku-band/5-beam radar system which is capable of operating in four different modes: radiometry, scatterometry, altimetry, and synthetic aperture radar.[4,13] We are particularly interested in the altimetry and SAR data types due to their high resolutions and geometric strengths. In the T8 Titan flyby, the first altimetry pass starts at P–32 minutes and ends at P–15 minutes ($\sim$ 17 minutes). The spacecraft then performs a small attitude maneuver and changes to SAR mode for about 30 minutes (i.e., up to P+15 minutes). During the last few minutes of the SAR surface scan, the spacecraft performs a small maneuver again to point toward nadir for altimetry, and during this back flip, the end portion of the T8 swath is observed over a longer period. The spacecraft then performs the second altimetry pass until P+32 minutes. The measurement schedule is illustrated in Figures 4 and 5.

C. Altimetry Model

As shown in Figures 4 and 5, when the spacecraft operates in altimetry mode, the radar transmits signals directly toward the nadir and measures the two-way time of flight between the spacecraft and the surface, and thus, in principle, can be considered as the usual range measurement:

$$\mathbf{z}_A \;=\; |\boldsymbol{\rho}| \;=\; \rho \tag{20}$$

where $\boldsymbol{\rho}$ is the vector from the spacecraft to the surface of Titan. The major error source of the altimetry measurement comes from the topographic elevation profile. We consider Titan as a spherical body with radius $R_T = 2575$ km and assume 50 meter accuracy for each altimetry measurement,[13] which is transmitted approximately every second. Also considering the slow (spin-locked) rotation rate of Titan (i.e., 15.95 day rotation period), we assume a stationary model. The measurement partial of the altimetry then yields[7,8]

$$\mathbf{H}_A \;=\; \frac{\partial \mathbf{z}_A}{\partial \mathbf{x}} \;=\; \left[\left(\frac{\partial \mathbf{z}_A}{\partial \mathbf{r}}\right)^T \quad \left(\frac{\partial \mathbf{z}_A}{\partial \mathbf{v}}\right)^T \right] \;=\; \left[\hat{\boldsymbol{\rho}}^T \quad \mathbf{0}_{1\times 3} \right] \tag{21}$$

D. Synthetic Aperture Radar Model

In practice, the SAR measurement is much more complex to process than the altimetry measurement. When the radar operates in SAR mode, the 4m high-gain antenna transmits a burst of radio waves and receives the reflected echoes from Titan's surface. Once the echoes are recorded, the on-board hardware translates them into corresponding range and Doppler bins. This information is then processed to create an image, called a *look*, where each pixel of a look corresponds to the range/Doppler pair. A series of bursts are processed to obtain multiple looks and are correlated to make swaths as shown in Figures 2 and 3. Hence, for navigational purpose, a SAR measurement is essentially a landmark on Titan's surface with associated range and Doppler values. Mathematically, the SAR/landmark measurement can be modeled as

$$\mathbf{z}_S \;=\; \left[\; \rho \,, \quad \hat{\boldsymbol{\rho}} \cdot \dot{\boldsymbol{\rho}} \;\right]^T \tag{22}$$

where $\hat{\boldsymbol{\rho}}$ is the unit position vector from the spacecraft to the landmark location. We note that the Doppler frequency shifts in the transmitted signals also provide angular information on the trajectory as well due to the Hamilton-Melbourne effect. The partial derivative of $\mathbf{z}_S$ results in

$$\mathbf{H}_S \;=\; \frac{\partial \mathbf{z}_S}{\partial \mathbf{y}} \;=\; \begin{bmatrix} \hat{\boldsymbol{\rho}}^T & \mathbf{0}_{1\times 3} \\ \dot{\boldsymbol{\rho}}^T \left(\dfrac{\partial \hat{\boldsymbol{\rho}}}{\partial \mathbf{r}}\right)^T & \hat{\boldsymbol{\rho}}^T \end{bmatrix} \tag{23}$$

where

$$\frac{\partial \hat{\boldsymbol{\rho}}}{\partial \mathbf{r}} \;=\; \frac{1}{\rho}\left(\mathbf{I}_{3\times 3} - \hat{\boldsymbol{\rho}}\,\hat{\boldsymbol{\rho}}^T\right) \tag{24}$$

The measurement accuracies are assumed to be 50 meter for the SAR range and 10 mm/s for the SAR Doppler.

Unlike the Magellan spacecraft, the Cassini radar has the 5-beam antenna configuration, and during the SAR campaign, each beam points in a slightly different direction and scans offset swaths of Titan as

illustrated in Figure 6. In other words, overlapped landmark observations are available even though the successive time interval is relatively short (i.e., $\sim$ 20 seconds). However, we later show that this offset configuration is important and improves the landmark estimation. Moreover, in order to emulate the T8 SAR swath (Figure 3), 12 pseudo-SAR/landmark measurements are created and are shown in Figures 4 and 5. Note that solid lines from the trajectory to the landmarks in Figure 5 represent the SAR measurements, and the offset beam configuration and the long observation of the last landmark are shown as well.

E. Landmark Uncertainty Model

Considering the SAR/landmark measurements, each landmark location vector must be estimated and the state to be estimated yields $\mathbf{p} = \mathbf{0}$ and $\mathbf{q} = \mathbf{r}_L^i$, where each landmark vector is defined as

$$\mathbf{r}_L^i = \begin{bmatrix} x_L^i & y_L^i & z_L^i \end{bmatrix}^T \tag{25}$$

for $i \in \{1, \cdots \kappa\}$. Here, κ is the number of landmarks, and for each landmark, we assumed initial uncertainties of 50 km in local planar and 1 km in radial directions. For each landmark, the uncertainties can be transformed into the Cartesian coordinate system by applying

$$\mathbf{P}_L = \mathbf{S} \begin{bmatrix} (1 \text{ km})^2 & 0 & 0 \\ 0 & (50 \text{ km}/R_T)^2 & 0 \\ 0 & 0 & (50 \text{ km}/R_T)^2 \end{bmatrix} \mathbf{S}^T \tag{26}$$

where S is the linear transformation matrix from the spherical coordinate system to the Cartesian frame. Hence the epoch landmark uncertainties yield $\sqrt{(\mathbf{P}_L)_{jj}}$ for $j \in \{1, 2, 3\}$.

To estimate the landmark location vectors, the only additional information required is the partials of the observation vector with respect to $\mathbf{r}_L^i$. Since we assume a stationary Titan the measurement partials simply yield

$$\frac{\partial \mathbf{z}_A}{\partial \mathbf{r}_L^i} = -\hat{\boldsymbol{\rho}}^T \tag{27}$$

and

$$\frac{\partial \mathbf{z}_S}{\partial \mathbf{r}_L^i} = \begin{bmatrix} -\hat{\boldsymbol{\rho}}^T \\ -\frac{\dot{\boldsymbol{\rho}}^T}{\rho} \left(\mathbf{I}_{3\times 3} - \hat{\boldsymbol{\rho}} \hat{\boldsymbol{\rho}}^T \right) \end{bmatrix} \tag{28}$$

IV. Simulation Results

As a baseline case, we assume 1000 measurements are obtained from each altimetry pass and 12 SAR/landmark observations are obtained from the T8 SAR swath. Also, considering the beam offset and spacecraft back flip, we assume that each landmark is observed twice with 20 second elapse time and the last landmark is observed three times over a 2 minute period. Figures 7 and 8 show the 1-σ state uncertainties as functions of time. From both plots we see that the SAR/landmark observation contribute no significant impact on the state estimation whereas the altimetry data alone provide about an order of magnitude improvement in the planar arc and in the along-track velocity direction (i.e., σ_{u_o}). Note that $[x_o, y_o, z_o]$ and $[u_o, v_o, w_o]$ are in Cartesian coordinate frame, but because of the small inclination from the equator, z_o and w_o can be considered as cross-track components. This indicates that the landmark errors must be reduced in order to draw any meaningful information contents for the state estimates. Table 2 shows the state *a posteriori* results considering individual data arc. The SAR only result confirms the importance of reducing the landmark errors. Also, Table 3 shows the level of accuracies of the landmark location vectors from the baseline simulation.

Next, the effectiveness of the beam offset is shown in Table 4, which is modeled by varying the measurement elapse time. The result shows that, although the state estimates are not affected, the 20-second delay between the successive SAR observation yields more than an order of magnitude improvement in landmark estimates. Hence the 5-beam configuration is an important advantage and can benefit both the state and landmark estimates than a single beam antenna.

Table 2. Spacecraft state *a posteriori* uncertainties

Cases	σ_{x_0} (m)	σ_{y_0} (m)	σ_{z_0} (m)	σ_{R_0} (m)	σ_{u_0} (mm/s)	σ_{v_0} (mm/s)	σ_{w_0} (mm/s)	σ_{V_0} (mm/s)
a priori	100	100	100	173.21	10	10	10	17.32
Altimetry 1 only	17.99	29.28	99.98	105.72	9.37	9.72	10	16.80
Altimetry 2 only	36.45	36.45	99.98	112.49	8.54	9.74	10	16.37
Altimetry 1 and 2	11.47	18.06	99.98	102.24	2.57	9.66	10	14.14
SAR only	100	99.92	99.98	173.15	9.98	10	10	17.31
Baseline	11.47	18.06	99.96	102.22	2.57	9.66	10	14.14

Table 3. Landmark nominal position, *a priori* uncertainty, and *a posteriori* uncertainty values

	Landmarks	x_L (km)	y_L (km)	z_L (km)	Landmarks	x_L (km)	y_L (km)	z_L (km)
Nominal	No. 1	-1631.20	1887.28	-638.73	No. 7	815.39	2402.50	-440.17
a priori		37.54	33.04	48.44		46.73	17.81	49.26
a posteriori		1.01	0.99	8.75		0.0090	0.036	0.75
Nominal	No. 2	-1289.29	2153.68	-574.48	No. 8	1216.34	2223.76	-453.92
a priori		42.21	26.81	48.74		43.39	24.87	49.22
a posteriori		0.70	0.59	7.14		0.034	0.038	0.42
Nominal	No. 3	-902.67	2354.50	-521.64	No. 9	1578.47	1976.74	-481.22
a priori		45.86	19.9	48.96		38.83	31.52	49.12
a posteriori		0.46	0.34	6.27		0.077	0.081	0.39
Nominal	No. 4	-484.64	2482.78	-481.22	No. 10	1889.70	1669.59	-521.64
a priori		48.24	13.18	49.12		33.30	37.31	48.96
a posteriori		0.30	0.22	6.78		0.17	0.23	0.54
Nominal	No. 5	-49.30	2534.20	-453.92	No. 11	2139.51	1312.66	-574.48
a priori		49.21	8.92	49.22		27.22	41.95	48.74
a posteriori		0.29	0.60	29.57		0.34	0.63	0.87
Nominal	No. 6	388.84	2507.13	-440.17	No. 12	2319.35	918.29	-638.73
a priori		48.70	11.37	49.26		21.25	45.27	48.44
a posteriori		0.038	0.064	2.57		0.077	0.17	0.20

Table 4. Landmark No.7 *a posteriori* uncertainties considering different beam elapse times

Elapse time (sec)	*a posteriori* x (km)	*a posteriori* y (km)	*a posteriori* z (km)
a priori	46.73	17.81	49.26
1	0.065	0.34	14.07
10	0.0097	0.047	1.48
20	0.0090	0.036	0.75
30	0.0090	0.034	0.52

Lastly, in order to simulate the importance of the SAR swaths overlap after a long time interval, we consider cases with reduced *a priori* landmark uncertainties:

- Case 1: landmark uncertainties of 75 m in the local planar directions and 2 m in the radial direction.
- Case 2: landmark uncertainties of 1 m in the local planar directions and 0.1 m in the radial direction.

As shown in Table 5, once the landmark uncertainties are known precisely, the out-of-plane motion uncertainty is improved and the significance of the SAR data becomes evident. We also note that processing the SAR/landmark data provides information, such as the Titan rotation model parameters, that are not available from the altimetry passes.

Table 5. Spacecraft *a posteriori* state uncertainties

	σ_{x_0} (m)	σ_{y_0} (m)	σ_{z_0} (m)	σ_{R_0} (m)	σ_{u_0} (mm/s)	σ_{v_0} (mm/s)	σ_{w_0} (mm/s)	σ_{V_0} (mm/s)
a priori	100	100	100	173.21	10	10	10	17.32
Case 1	11.25	17.80	56.29	60.10	2.46	9.59	9.70	13.86
Case 2	8.51	14.14	25.77	30.60	1.87	7.28	9.01	11.73

V. Conclusion

In this study, we have explored a possible use of the altimetry and SAR data as additional navigation observables for the Cassini Titan flybys. The T8 Titan flyby was considered as the nominal trajectory and the baseline result showed that processing the altimetry data alone can improve the spacecraft planar motion by an order of magnitude. Also discussed is the advantage of the 5-beam antenna, which is shown to improve the landmark estimation. Moreover, when landmarks are observed over a long time interval, which is simulated by assuming reduced landmark uncertainties, the SAR data become effective and can improve the spacecraft out-of-plane motion.

VI. Acknowledgement

The research described in this paper was carried out at the Jet Propulsion Laboratory, California Institute of Technology, as a part of the summer internship project. The authors would like to thank W.T.K. Johnson, B.W. Stiles, and R. West from the Cassini radar team at the Jet Propulsion Laboratory for their helpful comments and suggestions.

References

[1]Mohan, S. and Ananda, M., "SAR: An Instrument for Planetary Geodesy and Navigation," *Journal of the Astronautical Sciences*, Vol. XXIX, No. 2, April-June 1981, pp. 127–151.

[2]Chodas, P., Wang, T.-C., Sjogren, W., and Ekelund, J., "Magellan Ephemeris Improvement Using Synthetic Aperture Radar Landmark Measurements," *Astrodynamics Specialist Meeting*, August 1991, Durango, CO, AAS 91-391.

[3]Chodas, P., Lewicki, S., Hensley, S., and Masters, W., "High-Precision Magellan Orbit Determination for Stereo Image Processing," *Astrodynamics Specialist Meeting*, August 1993, Victoria, B.C., AAS 93-603.

[4]Website: Cassini Titan Flybys, http://saturn.jpl.nasa.gov/.

[5]Maybeck, P., *Stochastic Models, Estimation, and Control. Vol 1*, Republished by Navtech Book & Software Store, 1994, pp. 59−132.

[6]Maybeck, P., *Stochastic Models, Estimation, and Control. Vol 2*, Academic Press, 1982, pp. 159−271.

[7]Longuski, J., Fischbach, E., Scheeres, D., Giampieri, G., and Park, R., "Deflection of Spacecraft Trajectories as a New Test of General Relativity: Determining the PPN Parameters β and γ," *Phys. Rev. D*, Vol. 69, No. 042001, 2004, pp. 042001–1–042001–15.

[8]Park, R., Scheeres, D., Giampieri, G., Longuski, J., and Fischbach, E., "A Test of General Relativity: Estimating the Parameterized Post-Newtonian Parameters from Spacecraft Radiometric Measurements," *Journal of Spacecraft and Rockets*, Vol. 42, No. 3, 2005, pp. 559–568.

[9]Montenbruck, O. and Gill, E., *Satellite Orbits*, Springer, 2nd ed., 2001, pp. 257−291.

[10]Battin, R., *An Introduction to the Mathematics and Methods of Astrodynamics*, AIAA Education Series, AIAA, revised ed., 1999, pp. 623−698.

[11]Bierman, G., *Factorization Methods for Discrete Sequential Estimation*, Academic Press, 1977, pp. 69-76.

[12]Website: JPL HORIZONS system, http://ssd.jpl.nasa.gov/.

[13]Kirk, R., Callahan, P., Seu, R., Lorenz, R., Paganelli, F., Lopes, R., Elachi, C., and the Cassini RADAR Science Team, "Radar Reveals Titan Topography," *36th Lunar and Planetary Science*, March 2005, League City, Texas, AAS 91-391.

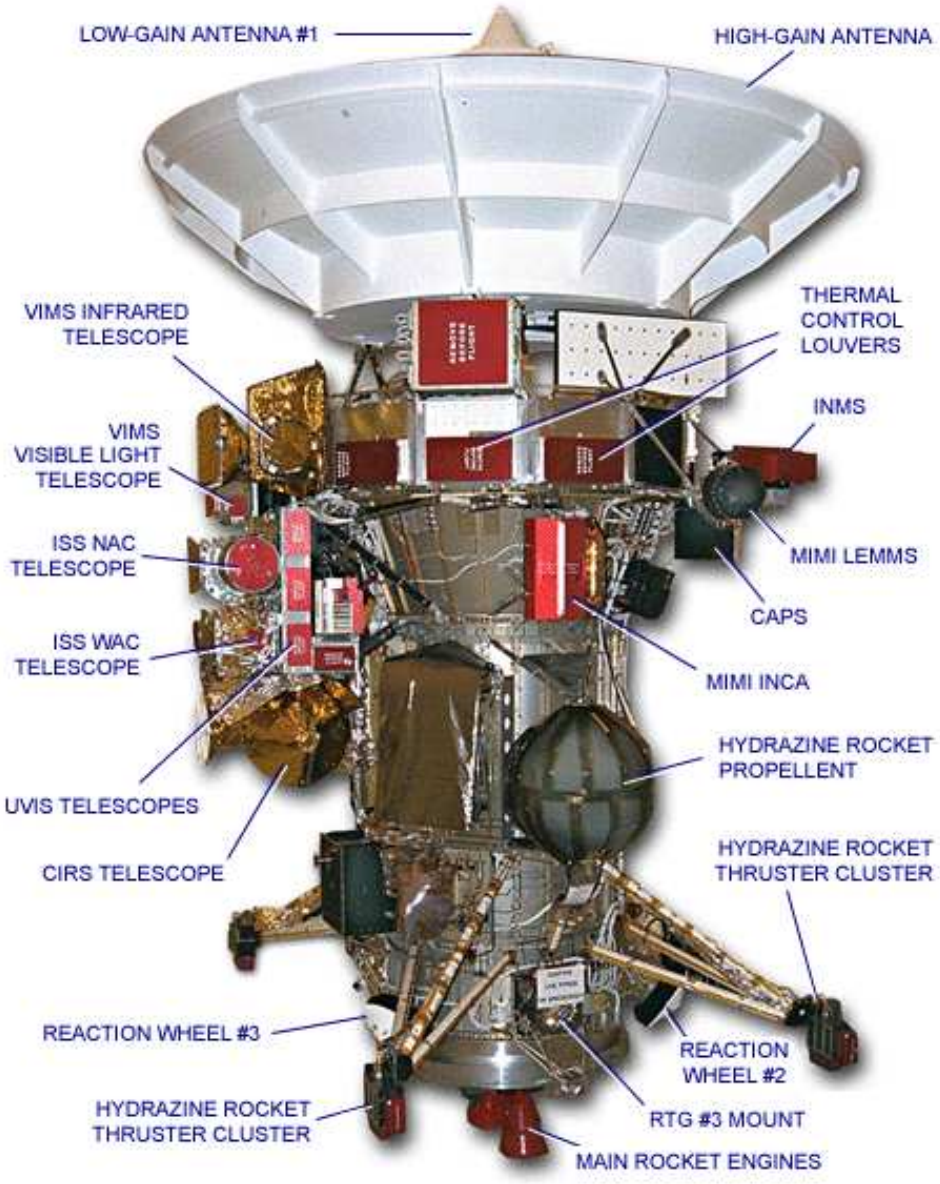

Figure 1. The Cassini spacecraft.[4]

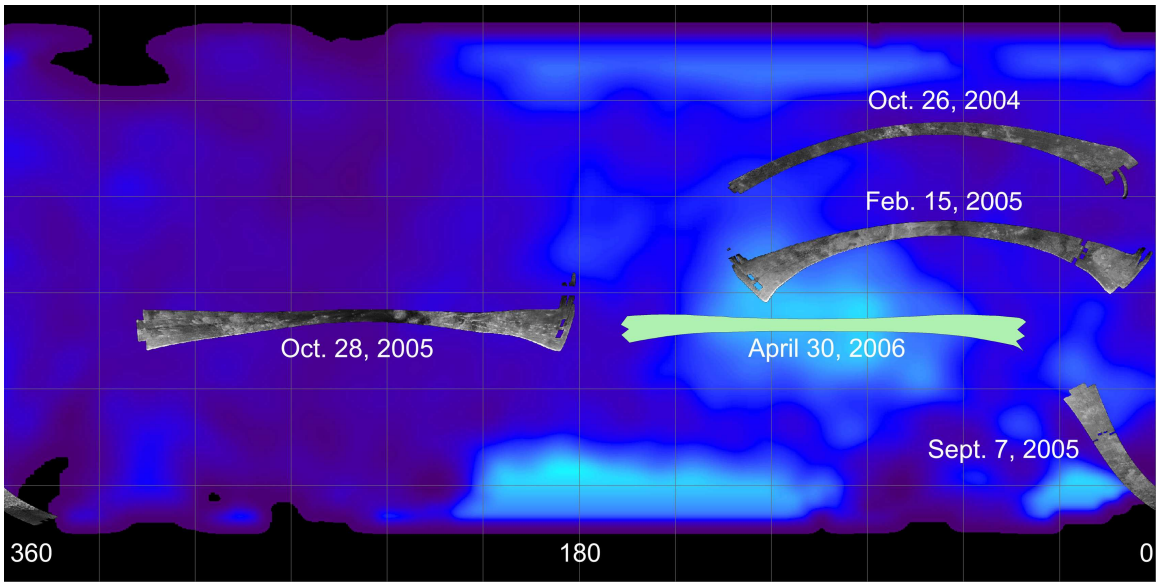

Figure 2. Available Cassini Titan flyby SAR swaths.[4]

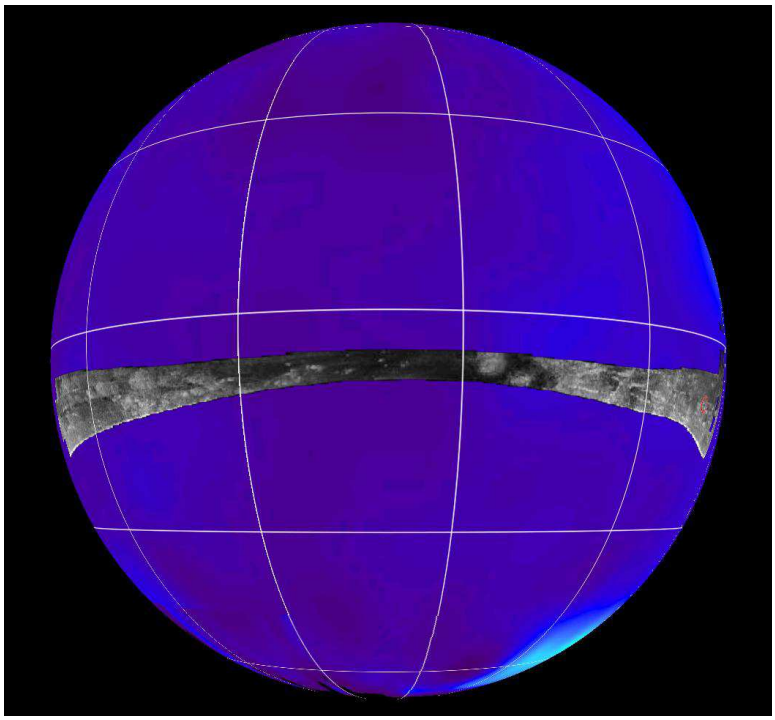

Figure 3. Cassini T8 (October 28, 2005) Titan flyby SAR swath.[4]

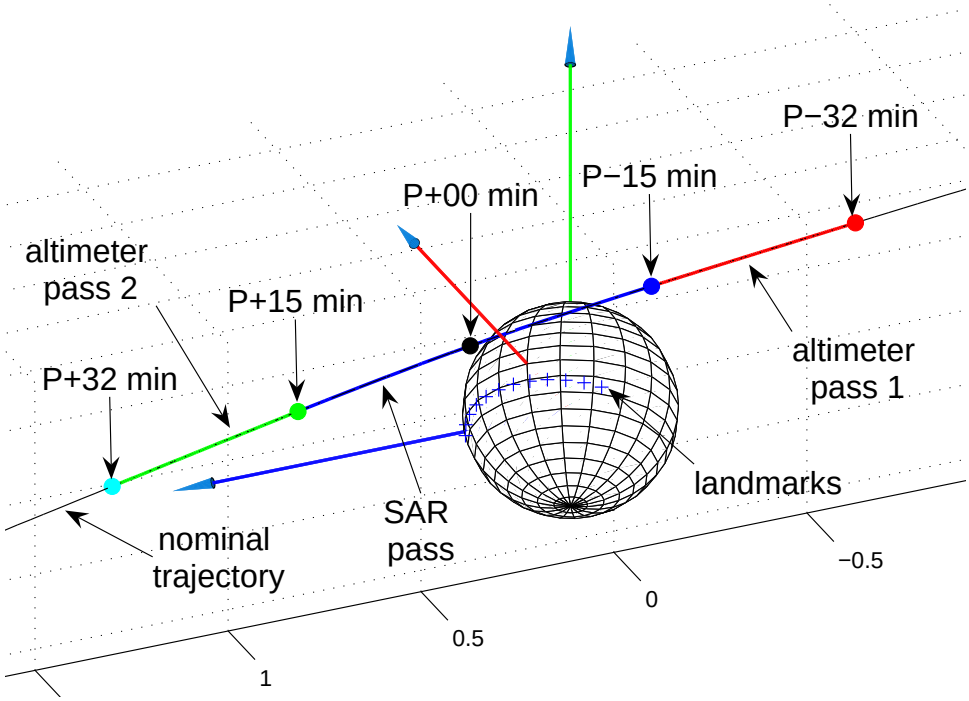

Figure 4. Cassini T8 Titan flyby nominal trajectory.

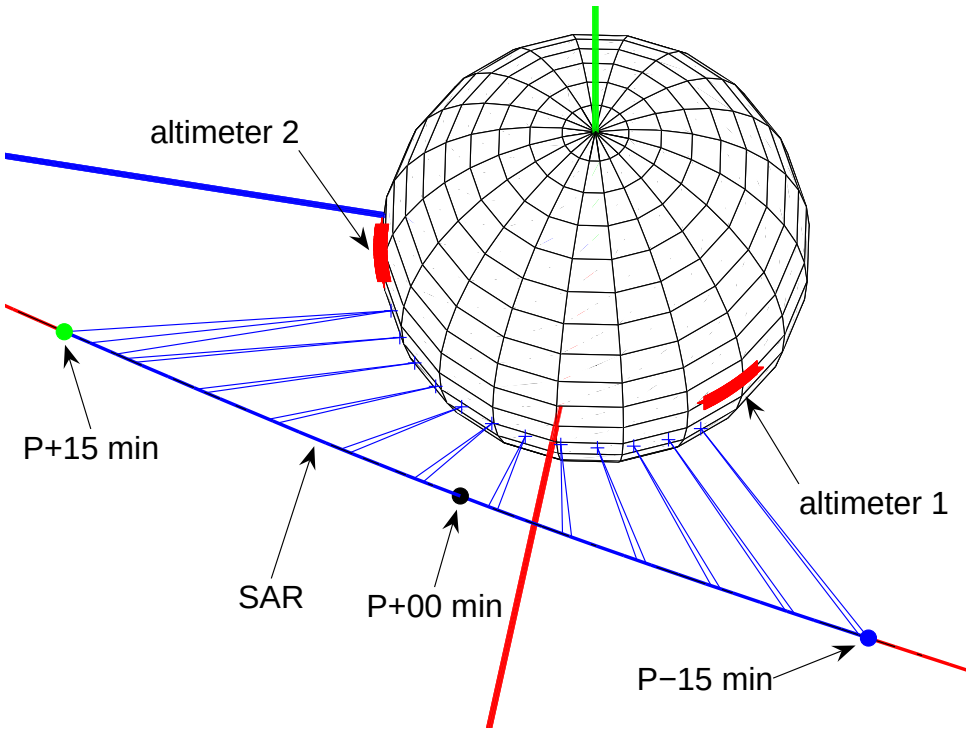

Figure 5. Cassini T8 Titan flyby nominal trajectory with baseline altimetry and SAR measurements.

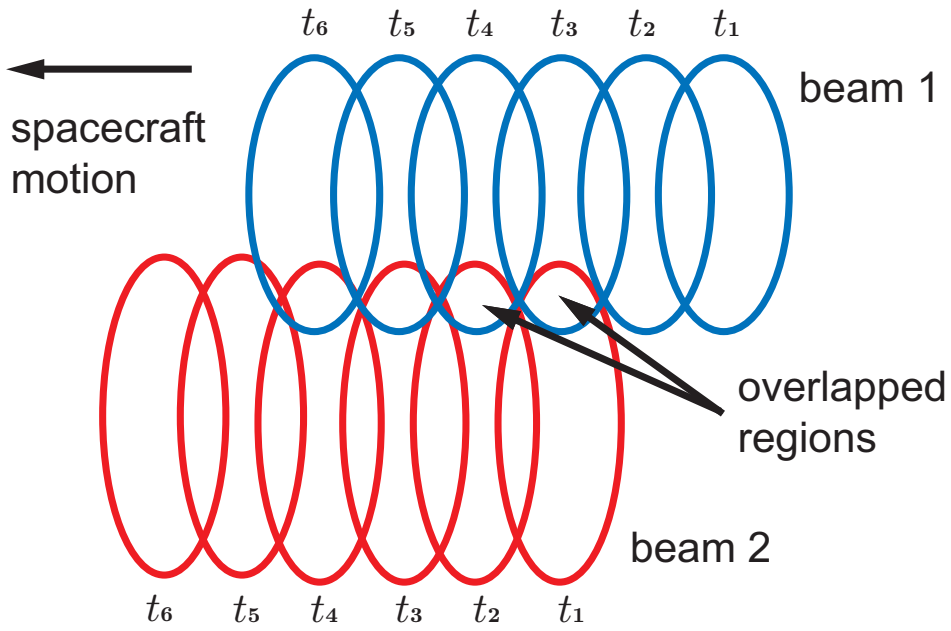

Figure 6. Illustration of the beam offset configuration (figure not in scale).

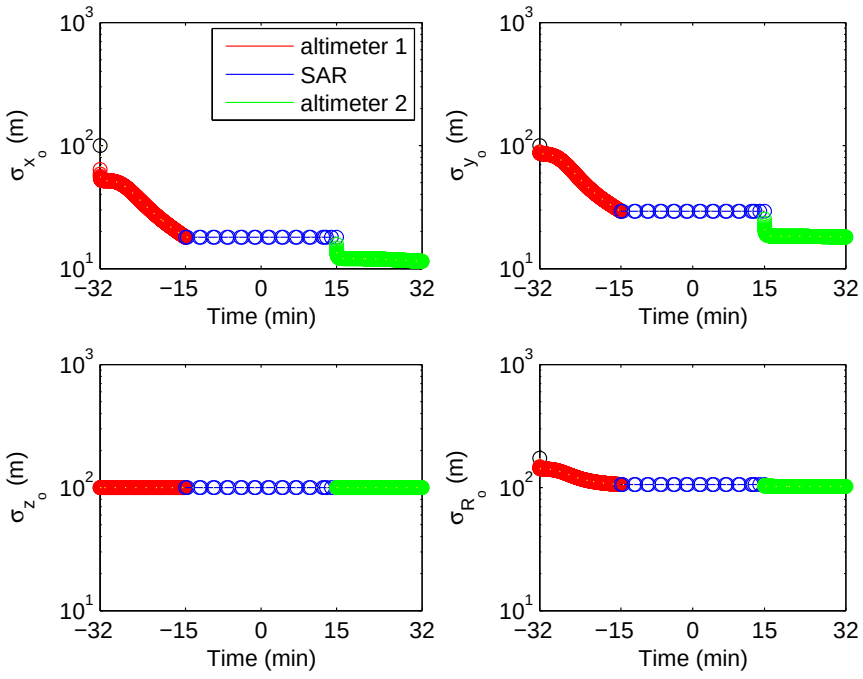

Figure 7. Baseline 1-σ position uncertainties as functions of time.

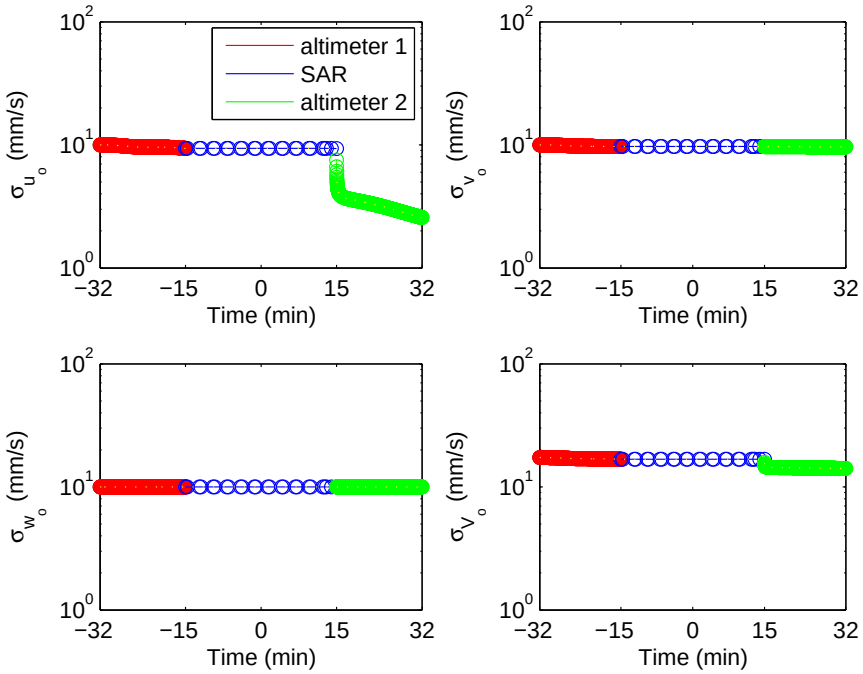

Figure 8. Baseline 1-σ velocity uncertainties as functions of time.